Solar Energy Advances 4 (2024) 100061

Contents lists available at ScienceDirect

Solar Energy Advances

journal homepage: www.elsevier.com/locate/seja

Performance improvement of hybrid photovoltaic/thermal systems: A metaheuristic artificial intelligence approach to select the best model using 10E analysis

Armel Zambou Kenfack [a,*], Modeste Kameni Nematchoua [a], Elie Simo [a], Venant Sorel Chara-Dackou [a,b], Boris Abeli Pekarou Pemi [a]

[a] Energy and Environment Laboratory, Department of Physics, Faculty of Science, University of Yaoundé I, P.O. Box 812, Cameroon
[b] Carnot Energy Laboratory(CEL), Department of Physics, Faculty of Science, University of Bangui, P.O. Box 1450, Bangui, Central African Republic

ARTICLE INFO

Keywords:
GA/MOPSO
Simplified modeling
10 E analysis
Comparative study
PV/T optimal model

ABSTRACT

Photovoltaic/thermal (PV/T) hybrid systems have until now encountered a real problem of sustainability-energy-cost concordance. Faced with this situation, new types of designs are in full expansion aimed at filling the limits of some. This therefore involves a very appropriate decision-making process. The energy, exergy, economic, environmental, energo-environmental, exergo-environmental, enviro-economic, energy-enviro-economic, exergo-enviro-economic and ergonomic analysis is carried out on seven PV/T configurations and therefore the simplified models are presented for a better interpretation of the mechanisms from different perspectives and the integration of a selection algorithm. Thus, an optimal selection methodology using the hybridization of genetic algorithms and multi-objective optimization by particle swarms based on ten performance indicators is proposed. The results obtained with good convergence and precision allow us to observe that the Air PV/T model is better. However, the study shows good viability of PV/T models with a cost of energy and a return on investment time all lower than 0.1$/kWh and 3 years, respectively. Models with phase change materials (PCM) minimize thermal losses better than those with air, nanofluids or thermoelectric generator (TEG). The bifacial model stands out with a good energy-environmental balance compared to the water model which has a better durability index greater than 2.0 and a good ergonomic factor.

1. Introduction

The availability of cheaper, clean and reliable energy is a major concern globally. It is therefore necessary to turn to renewable energies. As an alternative, solar energy is an intermittent source because it depends on weather conditions [1]. For its operation, we have photovoltaic (PV) panels and thermal sensors which directly produce electrical and thermal energy respectively. The heating of the PV cells, which lowers the power by 0.44 %/ °C, led researchers to combine the two systems into a single system [2]. Hybrid photovoltaic-thermal (PVT) systems combine both the photovoltaic conversion of solar energy into electricity and the use of solar heat for heating or hot water production [3]. However, the choice of cooling technologies (air, liquid, phase change materials, etc.) has a significant impact on the thermal and electrical performance of the PV/T system. The in-depth analysis of the physical and thermodynamic mechanisms governing these different configurations is essential to optimize the performance of PV/T systems. In this context, the use of a 10E analysis approach based on metaheuristic artificial intelligence aims to identify the best compromise in terms of energy efficiency, environmental impact, and reduced costs, thus highlighting the interest of air-based PV/T solutions despite their slightly lower performance compared to other technologies. These systems offer an efficient and versatile solution for optimally exploiting

Abbreviations: AI, artificial intelligence; AHP, analytical hierarchy process decision; AV, availablity; GA, genetic algorithm; COE, cost of energy; CPBT, cost payback time; EF, ergonomic factor; EXP, experimental; ENEV, energo-environmental; EXEV, exergo-environmental; P, packing factor; MOO, multi-ojective optimzation; MAE, mean absolute error; NF, nanofluids; NPV, net present values; NP, nanoparticule; TE, emission rate; TOPSIS, technique for order preference by similarity to ideal solution; RE, relative errror; TW, treated water; TAC, total annuel cost; EVEC, enviro-economic; ENEVEC, energo-environmental-economic; EXEVEC, exergo-environmental-economic; PV/T, photovoltaic/thermal; PCM, phase change matérial; SI, sustainability indice; TNF, ternary nanofluid.

* Corresponding author.
E-mail address: armelzambou199@gmail.com (A.Z. Kenfack).

https://doi.org/10.1016/j.seja.2024.100061
Received 24 April 2024; Received in revised form 11 June 2024; Accepted 11 June 2024
Available online 12 June 2024

Nomenclature

A	surface, m^2
C	specific heat, J $kg^{-1}K^{-1}$
D	diameter, m
d	diamètre de l'atome
G	solar radiation, W/m^{-2}
h	heat transfer coefficient, W/ m^{2}K
L	length, m
l	Largeur du nanowire
M	mass, kg
$\dot{m}$	mass flow rate, kg/m^3
E_x	exergy
T	temperature, °C
t	time, h
Ra	Rayleigh number
N_u	Nusselt number
N	number of tubes
h	Largeur du nanofilm
W	spacing of tubes, m
σ	Stephan Bolzmann constant W/m^{-2}K^{-4}

Subscripts

a	ambiant
c	convection
bf	basefluid
cond	conduction
ex	exergy
o	out
f	fluid
pv	PV module
p	absorber plate
r	radiation
i	insulation
el	electrical
th	thermal
nf	nanofluid
t	tube
s	sun

Greek symbols

α	absorbtivity
β	angle of inclination
β'	volumetric coefficient of expansion
δ	thickness
ε	emissivity
η	efficiency
ρ	density
τ	transmissivity
ϕ	volume concentartion

solar energy. Several studies have been conducted to evaluate the performance and benefits of PVT systems. A review of the literature reveals that these systems offer higher efficiencies compared to stand-alone photovoltaic or thermal systems [4]. In terms of design and configuration of PVT systems, different mathematical approaches have been studied. This includes the use of active and passive cooling systems. This multiplicity of models must be globally analyzed taking into account the energy, exergy, environmental, economic (4E) aspect and much more a combination.

Recently, authors such as Aruldoss et al. [5] performed a 4E analysis on a thermoelectric generator (TEG). The principle of TEG, using the Seebeck effect, where a difference in temperature of the layers, one connected to the back of the PV cells, causes the flow of current in the circuit. Their study aimed at producing drinking water and surplus electricity in an environmentally friendly manner. The system was found to be more expensive by $0.116/L for higher performance of the double-corner hybrid solar still compared to the passive system. Further, coupling of TEGs to a forced air and water pipe was carried out by Amirhooshang et al. [6], which showed a more efficient performance than the system with single TEG. Researchers have developed a PV module capable of absorbing solar flux simultaneously on the upper and lower sides. This causes a more considerable destroyed exergy in the system [7]. This deficiency is overcome by the use of paraffin wax phase change materials (PCM). Showing a significant evolution in performance. The PCMs are generally placed at the rear of the module. They thus absorb heat and begin to melt, going from a solid state to a liquid state. This was further optimized with the use of nanofluids added after the PCM material. But higher costs are observed in throughput from the increase in material thickness compared to the stand-alone PCM system [8,9]. On the other hand, the bulk of these configurations mentioned above, even more so that an in-depth study on ergonomic analysis and the search for greater efficiency sometimes lead to the use of simple cooling systems using the water, air, nanofluids or even more vegetable or synthetic oils [10,11]. These nanoparticles can be combined, leading to ternary nanofluids. Their small sizes and temperature-dependent thermo-physical properties allow the PV/T system to achieve generally higher performances than air PV/T systems [12]. In fact, their increased thermal conductivity increases heat exchange and the exergy destroyed is reduced in the system [13]. For more optimal electrical performance, a reflector is used a few millimeters behind the PV module with identical front and rear layers due to the absorption of part of the solar flux behind the PV cells. The authors [14] evaluated the performance of a BPV/T-Air system. Their study reveals that BPV/T-Air systems generate approximately 40 % more electricity than that of conventional PV with little increase in cost [15]. The authors [16] had the same conclusions to the extent that these systems have a higher financial gain. Their experimental study revealed the optimal parameters of inclination angle, slope and installation heights leading to optimal performance. More in-depth analyzes are carried out by the authors of Ref. [17]. Nine performance indicators are applied but limited for the choice of an optimal air PV/T configuration. This methodology has enabled performance improvement and also decision-making. But their decision making is only limited to nine decision indicators and for only one type of active air cooling. Furthermore, a real selection algorithm is not presented.

Precisely, 4E and even 9E analyzes allow us to better evaluate and position ourselves on the choice of an optimal system. However, a selection algorithm is generally recommended for the selection of an optimal system. A few rare studies implement selection methods. Another optimization method called MCD (Multi-criteria Decision) was applied to different cooling system configurations. The criteria considered include costs, reliability, environmental impact and ergonomics [18]. By studying eight cooling methods described in the literature, an approach based on entropy weighting was used to assess the importance of each criterion. This MCD method makes it possible to select the cooling configuration which is closest to the ideal and which is least far from the negative criteria. A normalization of the decision matrix is carried out to compare the weights of the different criteria. The results showed that the iphon thermos systems are the most efficient. On the other hand, in Ref. [19], using a combination of artificial neural network and genetic algorithm, optimal design conditions in terms of thermodynamic and economic performance are presented. The goal is to reduce the structural complexity of liquid air energy storage by minimizing the amount of equipment required. Thus, an in-depth comparison is carried

out between five storage systems, including the proposed system, conventional liquid air energy storage and single-stage or double-stage expansion compressed air energy storage with reheat, in order to put highlight the specific characteristics of the proposed system. Other approaches, such as the AHP (Hierarchical Process Analysis) method, have notably been used to determine an optimal location area based on six meteorological criteria [20–23]. This approach made it possible to observe that 59.46 % of the area is not suitable for the installation of photovoltaic systems. Indeed, excellent suitability for the installation of photovoltaic systems was observed on 0.12 % of the total area of the province, while suitable suitability is present on 25.66 % of this area. On the other hand, this approach is sometimes noted to be subjective, because the attribution of weights and priorities to alternatives depends on individual judgments. An optimization method called MCD (Multi--criteria Decision) was used by the authors [24,25] to evaluate different cooling systems by taking into account several decision criteria. This, by choosing the alternative that comes closest to the ideal while moving away from negative results. An entropy weighting approach was used to determine the importance of each criterion. Thus, a standardization step was carried out to put the weights of the criteria on the same scale. The study found that the optimal alternatives are thermosyphon PV/Ts. Other techniques such as genetic algorithms have been shown to be very efficient in finding optimal solutions [26]. An genetic algorithm (GA) numerical model developed by the authors [27], based on a genetic

(a) (b) (c)

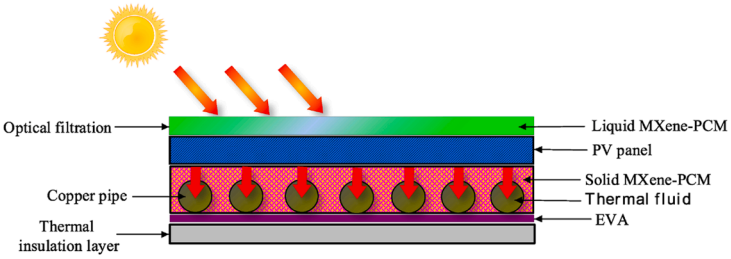

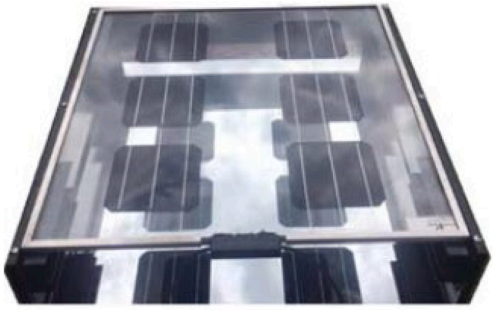

(d) (e)

231

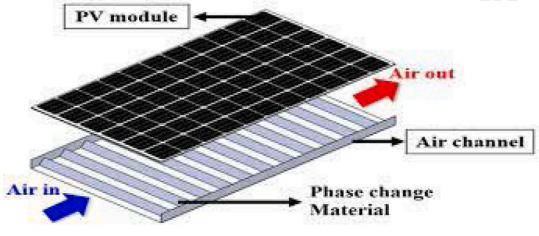

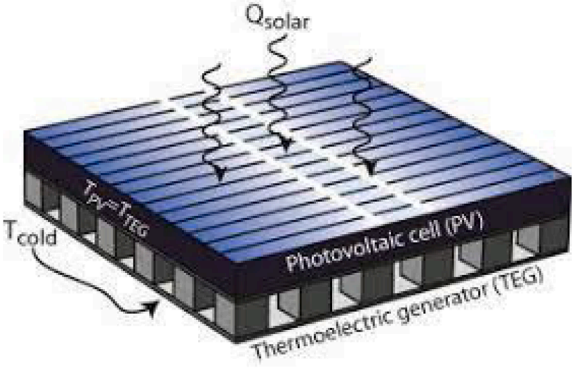

(f) (g)

. 1. Illustrations of the models of PV/T-Water (a), PV/T-Air (b), rear of PV/T-Water (c), PV/T-PCM/Liquid (d), BPV/T- Air (e), PV/T-PCM/Air (f), PV/T-TEG/Air (g) [31].

Fig. 2. Principle of energy conservation.

aggregation method, made it possible to provide an optimal mass flow by optimizing the Reynolds number with the objective functions of thermo-hydraulic performance, electrical efficiency and thermal. Despite the performance of this approach, GA optimization methods have drawbacks such as slow convergence. Indeed, GAs can be slow to converge to optimal solutions, especially in problems with large search spaces or expensive evaluation functions. Their performance depends heavily on parameters such as population size, crossover and mutation rates, which may require careful adjustments. Furthermore, they may converge prematurely towards sub-optimal local solutions if the diversity of the population is not preserved. On the other hand, particle swarm optimization (PSO), which draws its inspiration from the natural movements of animals such as birds and fish, has been shown to perform better. in decision making. To significantly improve the thermal performance of absorption systems, a recent study investigated the optimal design of a renewable energy system for five cities in the sub-Saharan region [28–30]. This system integrated different elements such as solar panels, wind turbines, hydroelectric turbines, energy storage systems and generators. The results obtained demonstrated that this method offered an effective management and development framework for hybrid solar systems, thus making it possible to resolve problems linked to the energy deficit with optimal choices. Likewise, the MOPSO (Multi-Objective Particle Swarm Optimization) method has disadvantages such as sensitivity to parameters, just like AG, MOPSO can be sensitive to parameters such as population size, attraction coefficients, etc. which requires appropriate adjustment. Also, Difficulty in handling extended Pareto fronts: MOPSO may encounter difficulty in handling extended Pareto fronts, where many non-dominated solutions exist, which may lead to less efficient convergence. The GA is therefore necessary for MOPSO because before searching for the optimal PV/T, it takes into account each model in its highest performances and under the same operating conditions. Thus, the advantage of GA/MOPSO hybridization can be summarized as follows [20,21] :

- Combination of the advantages of the two methods: The GA/MOPSO hybrid combines the exploration capabilities of GA and the balance between diversity and convergence of MOPSO;
- The ease of implementing the MOPSO method and the robustness of the genetic algorithm make the hybridization of the two methods easy to understand and find quality solutions;
- Convergence Improvement: By combining genetic operations with swarm update mechanisms, the GA/MOPSO hybrid can improve convergence toward optimal solutions.

To the authors' knowledge of previous studies, no selective model of the optimal PV/T system actually exists in the literature. The reference model [31] presents limitations in terms of variables used, which results in a failure to take into account certain system costs. Additionally, advances in cooling techniques such as thermoelectric generators, nanofluids, PCMs, and bifacial photovoltaic modules were not included in the database. The choice of criteria and their weighting can also lead to unreliable results. While the hybrid GA/MOPSO approach can offer better consideration of interactions between functions, thereby reducing subjectivity in decision-making. This approach presents satisfactory convergence and improved accuracy, while requiring less calculation time. It is important to note that no specific evaluation of PV/T models was performed using the GA/MOPSO meta-heuristic algorithm. However, it should be emphasized that the model in Ref. [31] does not fully consider all system costs, such as costs of piping, storage tank, heat exchanger, circuit breakers and inverter. Therefore, there is potential for improvement by including more precise optimal choices in the proposed solutions. In addition, many studies only deal with the energy aspect, which is insufficient for the optimization of the PV/T system. Few works present an exergy, environmental and economic analysis of this system; Even less an approach that combines its functions and for different PV/T configurations. In addition, with the variety of new PV module cooling geometries, a sophisticated technique aimed at choosing an optimal design of the PV/T system and taking into account ten performance indicators has not yet been the subject of 'a publication. This paper could therefore be justified by a comprehensive comparative analysis of the different cooling technologies (air, liquid, PCM, etc.) based on a representative set of case studies, and not just isolated results. To consider a range of evaluation criteria beyond just energy efficiency, such as durability, costs, environmental impact, etc. to obtain a global view of performance. To clearly identify the key conditions and parameters (climate, intended application, system size, etc.) that influence the relative advantages of the different technologies, rather than generalizing. Then to apply robust and validated analysis methods, such as the mentioned 10E analysis, on a diverse set of PV/T configurations to support the conclusions.

This study therefore has the main contribution:

- Seven simplified PVT hybrid system models are presented;
- The performances of seven PV/T models are evaluated;
- A 10E analysis of the different PV/T models is carried out;
- Optimization of a bifacial PV/T system;
- A numerical GA/MOPSO selection model is developed;
- An implementation of the hybrid GA/MOPSO model for the selection of the optimal PV/T.

These contributions will be structured into four main parts and therefore after the introductory section, will follow the second section entitled methodology, the third section entitled results and discussions and the fourth which concludes this study.

2. Methodology

2.1. Simplified mathematical models of configurations

These models will take into account the main equations governing the operation of the different PV/T systems. Fig. 1 presents practical illustrations of the different alternatives generally used and taken into account in this study. Notably Fig. 1.(a) to (g) is illustrated the system PV/T-Water, PV/T-Air, rear of PV/T-Water, PV/T-PCM/Liquid, BPV/T-Air, PV/T-PCM/Air, PV/T-TEG/Air, respectively. Given the complexity of its configurations, and to simplify their modeling, the following hypotheses are taken into account:

- The sky is considered as a black object with a temperature Ts;
- The temperatures are homogeneous across each layer of the PV/T system and the thermal characteristics of the different materials are constant;
- The circulation of fluids inside the tubes and the air passage spaces are forced and uniform in a single direction (x);
- The front and rear faces of the bifacial PV have the same characteristics;

- The PV/T-TNF and PV/TW configurations have the same physical geometry.

According to the principle of energy conservation, the energy balance of each configuration follows the path of Fig. 2. The diagram explaining the heat transfer mechanisms that take place is described in ref. [41].

2.1.1. Model PV/T-Fluids

This case includes configurations having cooling fluids circulating between the tubes. It explicitly concerns PV/T-Water and PV/T-TNF systems and implicitly PV/T-PCM/W, PV/T-PCM/Air, BPV/T-Air, PV/T-TEG/Air, PV/T-Air.

Energy balance at the Glass level

The glass cover, being directly exposed to the sun, is limited between the ambient air and the PV cells. According to the principle illustrated in Fig. 2, the energy balance, expressed in detail, applies to the glass layer. This is mathematically represented by Eq. (1). The glass of the envelope receives a flow of solar irradiation on its surface, leading to heat exchange by convection with the environment and the ambient air located below the glass. The heat flux absorbed by this layer is translated by the second term of the equation. In addition, the radiative flux passing through the glass is directed towards the PV cells. These aspects are represented by the last two terms of Eq. (1) [2,43].

$$\rho_g \delta_g C_g \frac{dT_g}{dt} = \alpha_g G + \left(h_{c,g-pv} + h_{r,g-pv}\right)\left(T_{pv} - T_g\right) - \left(h_{r,s-g} + h_{c,s-g}\right)\left(T_g - T_a\right) \quad (1)$$

The values of the radiative and convective heat transfer coefficients between the glass cover and the PV module, as well as between the glass cover and the environment, are represented by the expressions Eqs. (2)–(5) [4,24,35]. These coefficients describe the thermal exchanges that occur between the different surfaces involved

$$h_{c,g-pv} = \frac{N_u \lambda_a}{\delta_a} \quad (2)$$

$$h_{(r,g-pv)} = \frac{\sigma\left(T_g^2 + T_{pv}^2\right)\left(T_g + T_{pv}\right)}{\frac{1}{\varepsilon_g} + \frac{1}{\varepsilon_{pv}} - 1} \quad (3)$$

$$h_{(r,s-g)} = \frac{\sigma \varepsilon_g \left(T_g^4 - T_s^4\right)}{\left(T_a - T_g\right)} \quad (4)$$

$$\begin{cases} h_{(c,s-g)} = 3.8V + 5.7 \\ h_{(c,s-g)} = V^{0.78} + 6.47 \end{cases} Respectivelyfor\langle 5\ et\ V\rangle 5Vm \Big/ s. \quad (5)$$

Energy balance on PV cells

In the case of PV cells, the energy balance follows the same logic as that applied to the glass roof. Thus, Eq. (6) takes into account the heat flow that enters the PV cells and is limited by the glass cover and the absorber. The third term in the equation represents the convective and radiative heat exchange between the glass cover and the PV cells. Then, the fourth term characterizes the heat exchange by conduction between the PV cells and the absorber plate. The fifth term represents the electrical energy produced. There is no energy exchange with the outside in this layer [10].

$$\rho_{pv} \delta_{pv} C_{pv} \frac{dT_{pv}}{dt} = \alpha_{pv} \tau_g G + \left(h_{c,g-pv} + h_{r,g-pv}\right)\left(T_g - T_{pv}\right) + h_{cond,pv-p}\left(T_p - T_{pv}\right) - E_{elec} \quad (6)$$

The term $h_{cond,pv-p}$ is the transfer coefficient between PV module and absorber can be calculated from Eq. (7) [24].

$$h_{cond,pv-p} = \frac{1}{\left(\frac{\delta_{pv}}{K_{pv}} + \frac{\delta_p}{K_p}\right)} \quad (7)$$

Energy balance on the absorber plate

It is framed by the PV module and the tubes. Its heat balance is described by Eq. (8). This layer is mainly dominated by thermal conduction, as it is not directly exposed to solar radiation and there is no convective heat exchange due to the close contact with other surfaces [27].

$$\rho_p \delta_p C_p \frac{dT_p}{dt} = h_{cond,pv-p}\left(T_p - T_{pv}\right) + h_{cond,p-t}\left(T_t - T_p\right) + h_{cond,p-i}\left(T_i - T_p\right) \quad (8)$$

$h_{cond,p-t}$ and $h_{cond,p-i}$ represents, respectively the transfer coefficients respectively by conduction between the absorber and the tubes then between the absorber and the insulator given by the relations Eq. (9) and Eq. (10) [27].

$$h_{cond,p-t} = \frac{8\delta_p \mathrm{LK_p}}{\mathrm{A(W - D_o)}} \quad (9)$$

$$h_{cond,p-i} = \frac{2K_i}{\delta_i}\left(\frac{\mathrm{W - D_o}}{\mathrm{W}}\right) \quad (10)$$

Energy balance at tube level

Two types of heat transfer occur in this system. First of all, the heat propagates by conduction between the absorber and the tubes, as well as between the tubes and the insulator because they are in contact (Fig 1. d). In addition, there is heat exchange by convection between the tubes and the fluid. Eq. (11) represents the energy balance [29].

$$m_t C_t \frac{dT_t}{dt} = A_{pt} h_{cond,p-t}\left(T_t - T_p\right) + A_{tf} h_{c,t-f}\left(T_f - T_t\right) + A_{ti} h_{cond,t-i}\left(T_i - T_t\right) \quad (11)$$

Transfer coefficients by conduction and convection$h_{cond,t-i}$ and $h_{c,t-f}$ are, respectively given to Eq. (12) and Eq. (13) [30].

$$h_{cond,t-i} = \frac{2\mathrm{K_i}}{\delta_\mathrm{i}} \quad (12)$$

$$h_{c,t-f} = \frac{\mathrm{N_u K_f}}{\mathrm{D_i}} \quad (13)$$

Energy balance at the level of the heat transfer fluid

The first term in Eq. (14) corresponds to the amount of energy stored in the heat transfer fluid. The second term expresses the quantity of heat transferred to the fluid by the tubes. The third term represents the quantity of heat transferred to the heat transfer fluid through the addition of a mass of heat transfer fluid at a given temperature to the inlet of the collector, and through the extraction of this same mass of heat transfer fluid at a different temperature at the outlet [2].

$$m_f C_f \frac{dT_f}{dt} = A_{tf} h_{cond,t-f}\left(T_t - T_f\right) + \dot{m}_f C_f \left(T_{fo} - T_{fi}\right) \quad (14)$$

Energy balance on insulation

The insulation located under the PV/T collector is in contact with the tubes and part of the absorber, then with the ambient air. Its energy balance can therefore be expressed using Eq. (15) [4].

$$m_i C_i \frac{dT_i}{dt} = \mathrm{A_{ti}} h_{cond,t-i}\left(T_t - T_i\right) + \mathrm{A_{pi}} h_{cond,p-i}\left(T_i - T_p\right) - \mathrm{A} h_{c,i-a}\left(T_i - T_a\right) \quad (15)$$

$h_{c,i-a}$ And $h_{c,s-g}$ represents, respectively the transfer coefficient by convection between the insulation and the ambient air then between the sun and the glass cover [27].

2.1.2. Specific case for PV/T-Air

Its geometry is particularly simple, characterized by the absence of tubes [7]. It therefore follows the same path as the PV/TW model in the absence of tubes. However, in terms of the space reserved for air circulation, the results are different.

Energy balance at the air channel level

It is expressed by the expression of Eq. (16).

$$m_f C_f \frac{dT_f}{dt} = A\left(h_{c,pv-f}\left(T_{pv} - T_f\right) + h_{c,i-f}\left(T_i - T_f\right)\right) \tag{16}$$

2.1.3. Specific case for PV/T-PCM/W

It is particularly marked by the PCM layer. The energy balance is therefore identical to that of the PV/TW configuration by replacing the absorber plate with PCM materials.

Energy balance on the PCM

In place of the absorbent plate, the PCM material is placed. Its balance is therefore given by Eq. (17).

$$M\frac{dT_{pcm}}{dt} = h_{cond,pv-pcm}\left(T_{pcm} - T_{pv}\right) + h_{cond,pcm-t}\left(T_t - T_{pcm}\right) + h_{cond,pcm-i}\left(T_i - T_{pcm}\right) \tag{17}$$

The term M is a function of the PCM temperature given in Eqs. (18)–(20). [6–32]. And Eq. (21) represents the conduction transfer coefficient between the PCM and the insulator.

$$\text{For } T_{pcm} < T_m,\ M = m_{pcm} C_{s,pcm} \tag{18}$$

$$\text{For } T_{pcm} > T_m,\ M = m_{pcm} C_{l,pcm} \tag{19}$$

$$\text{For } T_{pcm} = T_m,\ M = m_{pcm} L_{pcm} \tag{20}$$

$$h_{cond,pcm-i} = A_{pcm}\left[\frac{\delta_{pcm}}{kpcm} + \frac{\delta_i}{ki}\right]^{-1} \tag{21}$$

2.1.4. Specific case for PV/T-PCM/Air

This configuration is less simple than the PV/T-PCM/W system. Instead of tubes, air is circulated behind the PCM materials. Thus, in the PV/T-PCM/W system model, the tubes are replaced by an air circulation space described previously in Eq. (16).

2.1.5. Specific case for PV/T-TEG/Air

The thermoelectric generator directly converts heat into electricity through the thermoelectric effect. The temperature difference between the front and back faces of thermoelectric materials generates an electric potential difference called the Seebeck effect [34]. Its mathematical model is identical to that of PV/TW, but replacing the absorbent plate layer with TEG materials and the tube part with the air circulation space.

The energy balance on TEG materials is expressed in Eq. (22):

$$\rho_{teg}\delta_{teg}C_{teg}\frac{dT_{teg}}{dt} = h_{c,teg-a}\left(T_a - T_{teg}\right) + h_{cond,pv-teg}\left(T_{teg} - T_{pv}\right) - E_{teg,elec} \tag{22}$$

With $E_{elec,teg}$representing the surplus of electrical energy produced by the TEG and expressed at Eq. (23) [2,3].

$$E_{elec,teg} = \eta_{te}\Delta T_{te}\left(2R_{te} + \frac{\delta_{te}}{k_{te}}\right)^{-1} \tag{23}$$

And ΔT_{te}represents the temperature difference between the front and back side of the TEG layer. The TEG conversion energy $\eta_{te}$is given by Eq. (24) [17]:

$$\eta_{teg} = \left(1 - \frac{T_{cold}}{T_{hot}}\right)\frac{\sqrt{1+ZT}}{\sqrt{1+ZT} + \frac{T_{cold}}{T_{hot}}} \tag{24}$$

where ZTis a dimensionless expression defined as a symbol for thermoelectric performance, given in Eq. (25) [5].

$$ZT = \frac{1}{T_{hot} - T_{cold}}\int_{T_{cold}}^{T_{hot}}\left(\frac{S^2}{\rho_e k_T}\right)dT \tag{25}$$

With S, $\rho_e$and $k_T$represents the Seebeck coefficient, resistivity and thermal conductivity respectively.

2.1.6. Case specific to BPV/T-Air

The BPV/T model used in this study consists of a white reflector, Fig. 1.e, allowing all rays passing through the glass cover and the PV module to be reflected back to the PV cells. Thus maximizing its production [31]. It therefore only consists of the glass collector, the PV module, the reflector and the insulator. Thus, the energy balance on the glass cover is identical to that of PV/TW.

Energy balance on the BPV module

The energy balance of the BPV having undergone lamination making it possible to bind the different front and rear layers together in a stable manner to optimize the capture of solar radiation. It is expressed by Eq. [26].

$$\rho_{bpv}\delta_{bpv}C_{bpv}\frac{dT_{bpv}}{dt} = \alpha_{bpv}\tau_g G + \left(h_{c,g-bpv} + h_{r,g-bpv}\right)\left(T_g - T_{bpv}\right) + h_{c,bpv-a}\left(T_a - T_{bpv}\right) - h_{r,R-bpv}\left(T_{bpv} - T_R\right) - E_{bpv,elec} \tag{26}$$

With $h_{r,R-bpv}$representing the radiation transfer coefficient between the BPV module and the reflector [15]. It is identical to the coefficient $h_{r,g-pv}$by replacing the terms g and pv by the terms R and bpv respectively.

Energy balance on the reflector

It is connected in direct contact with the insulation. Its energy balance is given by Eq. (27).

$$\rho_R\delta_R C_R\frac{dT_R}{dt} = h_{r,pv-R}\left(T_{pv} - T_R\right) + \dot{h}_{c,R-f}\left(T_R - T_f\right) + \dot{h}_{cond,i-R}\left(T_i - T_R\right) \tag{27}$$

The energy balance of the air channel is identical to that of Eq. (16) with the addition of a term representing the quantity of energy exchanged by convection $h_{c,\ f-R}\left(T_f - T_R\right)$ between the air fluid and the reflector [33].

2.2. Performance

Efficiency is an important aspect in evaluating the performance of an energy system. Its expression is given in Eq. (28) [18].

$$\eta_{en} = \frac{Q_u}{GA} \tag{28}$$

With $Q_u$representing the quantity of useful energy of the system and which varies depending on the configurations. It is generally expressed as in the expression Eq. (29).

$$Q_u = \dot{m}_f C_f\left(T_{fo} - T_{fi}\right) \tag{29}$$

For the case of PCMs, it is expressed in Eq. (30) [3].

$$Q_u = \dot{m}_f C_f\left(T_{fo} - T_{fi}\right) + m_{pcm}L_{pcm} \tag{30}$$

With m_{pcm}being the mass of the PCM which varies as a function of temperature expressed in Eq. (31) [6].

$$m_{pcm} = \frac{Q_{ch}}{L_F + \int_{T_a}^{T_m} C_{s,pcm}dT + \int_{T_m}^{T_f} C_{l,pcm}dT} \tag{31}$$

Where $Q_{ch}$is the heat channel of PCM

In the case of PV-TEG/Air systems, the quantity of electrical energy produced is given in Eq. (32) [17].

Table 1
Mathematical model of decision functions.

NPV	$NPV = \left(\frac{LCS}{i_d - i_i}\right)\left[1 - \left(\frac{1+i_i}{1+i_d}\right)^n\right] - C_i$	LCS	$LCS = \frac{(1+i_i)^{n-1}}{(1+i_d)^n}\left[C_{el}\sum_{month=1}^{12}(E_{el})_{month} + C_{th}\sum_{month=1}^{12}(E_{th})_{month}\right]$
TAC	$TAC = CRFC_i\left(1 + \frac{C_o}{C_i} - \frac{SV}{C_i}\right)$	CPBT	$CPBT = \frac{C_i}{C_{el} \times ((E_{el} \times 0.38) + E_{th})}$
EV	$EV = e \times \sum_{month=1}^{12}((E_{el} \times 0.38) + E_{th})_{month}$	IF	$IF = 1/(1- \eta_{ex,ov})$
EVEC	$EVEC = EV \times e_p$	COE	$COE = \frac{TAC}{\sum_{month=1}^{12}((E_{el} \times 0.38) + E_{th})_{month}}$
ENEV	$ENEV = e \times Q_u \times t_y$	ENEVEC	$ENEVEC = ENEV \times e_p$
EXEV	$EXEV = e \times Ex_u \times t_y$	EXEVEC	$EXEVEC = EXEV \times e_p$

$$\boldsymbol{Q_{elec}} = GA_c\eta_o[1 - \beta(T_c - T_a)] + E_{elec,teg} \quad (32)$$

For the BPV/T-Air system, the amount of electrical energy produced is given in Eq. (33) [16].

$$\boldsymbol{Q_{elec}} = G\,A_c\alpha_{pv}\eta_{pv}P(1 + \tau_L\eta_R(1 - P)) \quad (33)$$

The electrical and thermal efficiencies are, respectively given in the expression Eq. (34) and Eq. (35) [8].

$$\eta_{th} = \frac{Q_u}{G.A_c} \quad (34)$$

$$\eta_{el} = \frac{\boldsymbol{Q_{elec}} - \frac{m_f \times \Delta_p}{\rho_f \times \eta_{pump}}}{G.A_c} \quad (35)$$

The electrical energy being very close to that of electrical energy. It can be established that the total exergy efficiency of the system is the ratio of the useful exergy to the incoming exergy Eq. (36). The first represents the useful thermal exergy Ex_u. [9].

$$\eta_{ex,ov} = \frac{m_f \times C_f\left[T_{fo} - T_{fi} - ln\left(\frac{T_{fo}}{T_{fi}}\right)\right] + \boldsymbol{Q_{elec}} - \frac{m_f \times \Delta_p}{\rho_f \times \eta_{pump}}}{GA\left[1 - \frac{4}{3}\left(\frac{T_a}{T_s}\right) + \frac{1}{3}\left(\frac{T_a}{T_s}\right)^4\right]} \quad (36)$$

2.3. Mathematical model of decision functions

In this study, ten objective functions being more or less linked and falling within the energy, exergy, economic, environmental, energy-environmental, exergo-environmental, enviro-economic, energy-enviro-economic, exergo-enviro-economic and ergonomic. Their mathematical expressions are well detailed in Ref. [7]. Table 1 [7,12] summarizes their different expressions.

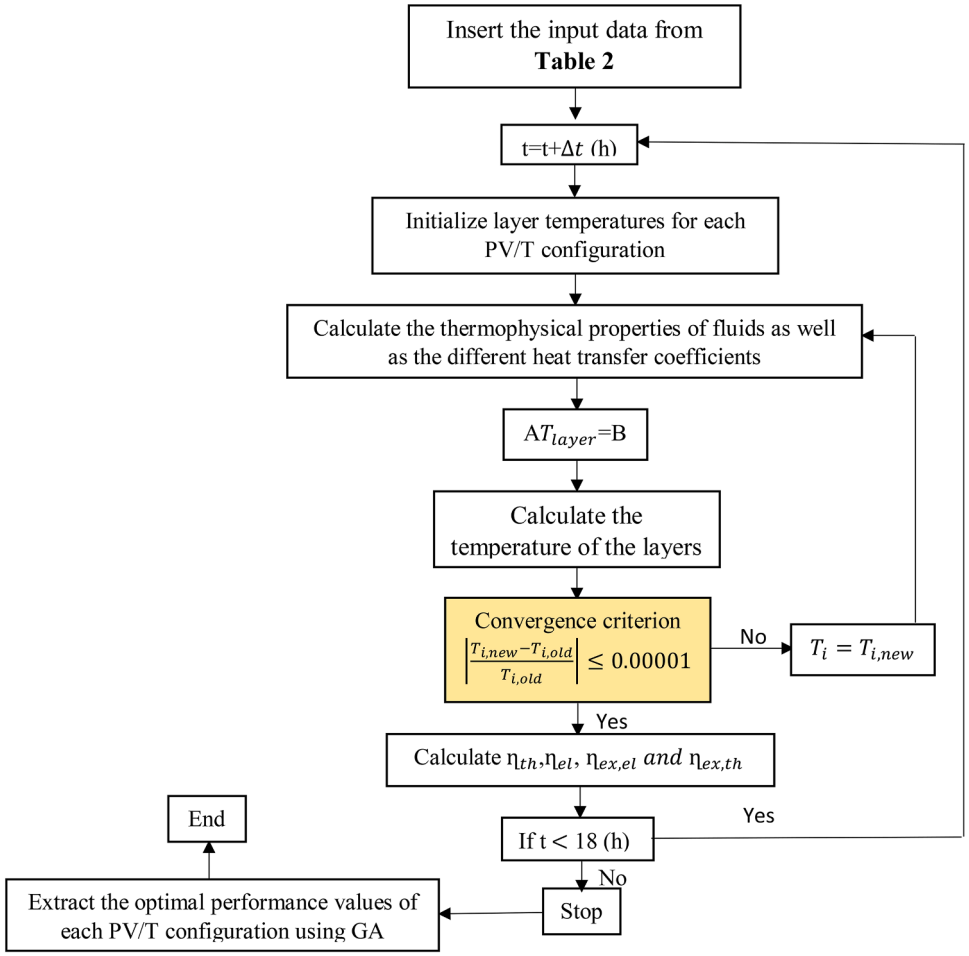

Fig. 3. Calculation flowchart.

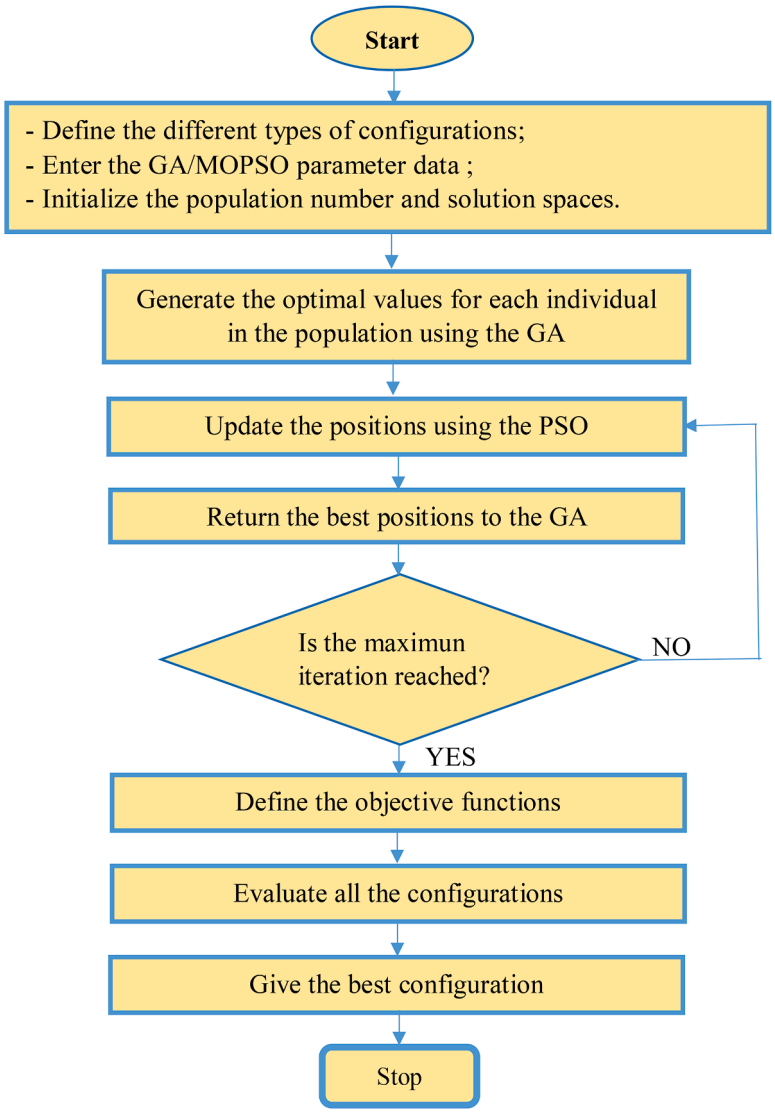

Fig. 4. Step of the GA/MOPSO method.

For the ergonomic factor (EF), it is based on the aspect of comfort and safety to minimize the size of the system. This is one of the problems faced by designers seeking to make the system accessible for maintenance [31]. Thus, depending on the number of equipment and their weight, the most ergonomic configurations are classified from PV/T-Air, BPV/T-Air, PV/T-TEG/Air, PV/T-TNFs, PV/T-PCM/W, PV/TW, PV/T-PCM/Air. This classification is influenced by the type of PCM materials, which are all identical (paraffin-based). The unit costs and lifespan of the different PV/T equipment can be found in Refs. [3,5,6, 41]. It should be noted that these prices take into account the export costs of these materials and are specific to a very low-income country, for globalization and so that it is favorable to any economic situation in any area. For the case of ternary nanofluids, the thermophysical properties are taken from Ref. [12].

2.4. Digital processes

2.4.1. Digital resolution

The mathematical models presented, which are coupled differential equations, are discretized. This is done using the finite difference method, which is represented by Eq. (37) to obtain the linear form. And then the Gauss-Seidel method is used for the numerical resolution [41, 43].

$$\frac{dT_{layer}}{dt} = \frac{T_{layer}^{t+\Delta t} - T_{layer}^{t}}{\Delta t} \tag{37}$$

By bringing together the various related balance sheet equations, they are expressed in the form AT=*B*. where A is a square matrix of coefficients, T is the vector of unknown variables and B is the vector of constant terms. Then, an iterative loop is adapted until convergence is reached as presented in the flowchart in Fig. 3.

To validate these models, Eq. (38) which represents the relative error [40,42] is used as a statistical indicator making it possible to check the difference with different studies in the literature.

$$RE = \frac{1}{n}\sum_{i=1}^{n}\left(\frac{|Sim - Exp|}{Exp}\right) \tag{38}$$

2.4.2. Optimization process

Multi-objective genetic algorithm Particle Swarm Optimization (GA/MOPSO) is a combination of two optimization techniques: genetic algorithm (GA) and multi-objective particle swarm optimization (MOPSO). This hybrid approach makes it possible to solve multi-objective optimization problems, that is to say problems where several objectives must be optimized simultaneously. This is one of the very promising techniques. The GA is used to take the optimal performance of

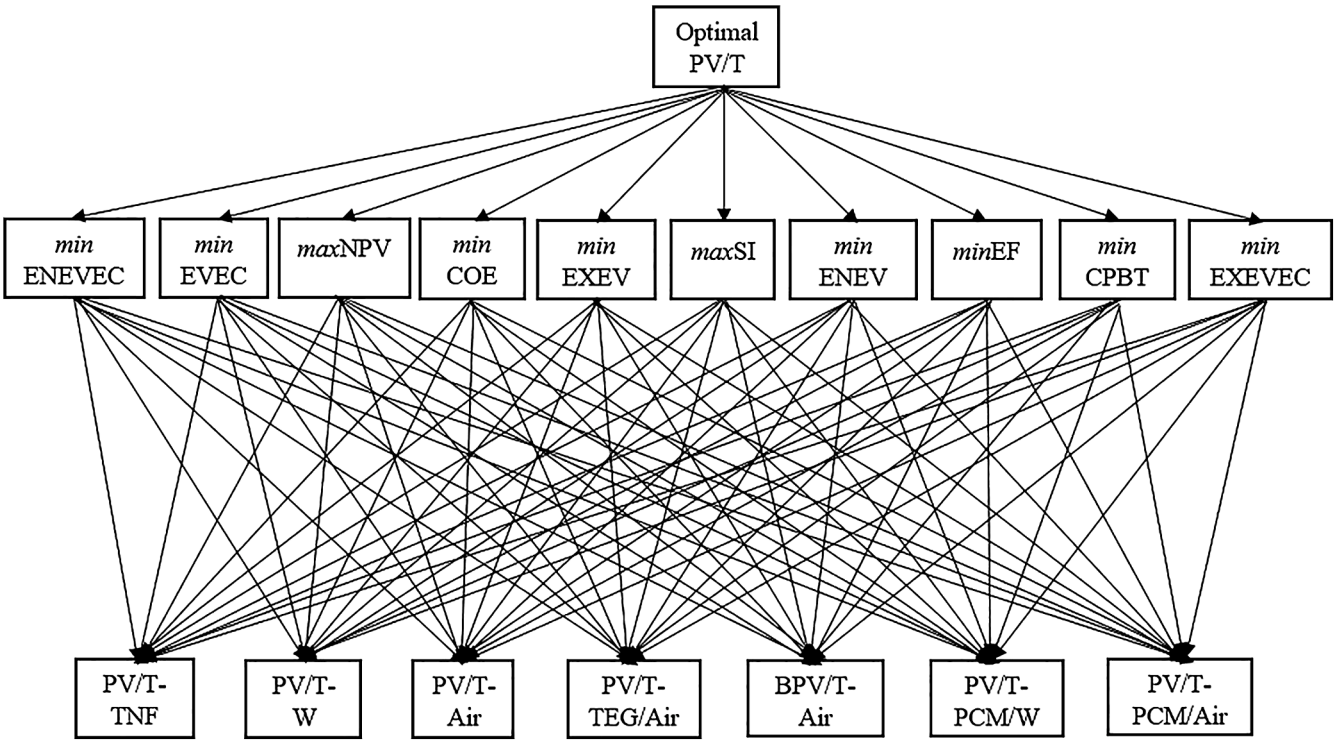

Fig. 5. Optimal selection network.

Table 2
Input data [13,21 and 25].

Rated power (Monocrystalline)	50W	K_{np}	8.9 W/mK
Type	Monocrystalline	ρ_g	0.78 kg/m^3
A	1.3m^2	ρ_{np}	4250 kg/m^3
C_{np}	686 J/kg K	ρ_p	2707 kg/m^3
C_g	670 J/kg K	ρ_t	8950 kg/m^3
C_i	670 J/kg K	ρ_i	20 kg/m^3
D	0.5m	σ	1.38 × 10^{-23} m^2kg.$s^{-2}K^{-1}$
Type of TNF	CuO-MgO-TiO_2	H	5.4nm
L	6.7nm	ε_g	0.88
K_i	0.034 W/mK	ε_p	0.05
K_g	310 W/mK	P	0.66
OM 37 melting point T_m	37 °C	K_{teg}	0.9 W/m K
L_{pcm}	211 kJ/kg	ρ_{teg}	92.74 kg/m^{-3}
$C_{s,pcm}$	2.2 J.kg/K	ρ_e	2.3622× $10^{-4}\Omega$
$C_{l,pcm}$	1.7 J.kg/K	C_{teg}	708.4 J/kg^{-1}K
Q_{ch}	100 J/kg	S	2.3×10^{-4} V.K^{-1}
τ_L	0.85	GA/MOPSO parameters	
η_R	0.7	Population size	100
$\rho_{l,pcm}$	770 kg/m^3	Mutation rate	0.1
$\rho_{s,pcm}$	880 kg/m^3	Number of iterations	
$K_{l,pcm}$	0.4 W/m K	Maximum speed	1.5
$K_{s,pcm}$	0.5 W/m K	Number of particles	75
R_{te}	10^{-4}K.m^2/W	c_1	1.8
L_F	228.9 KJ/kg	c_1	2

each configuration subject to the same characteristic, dimensional and meteorological operating conditions. And the MOPSO method makes it possible to have among the different configurations optimized thanks to AGs, the optimal configuration subject to several decision functions (Fig. 4). The GA/MOPSO algorithm generates a population of PV/T systems with different configurations. Each system is evaluated in terms using ten specific functions (10 $^{E)}$ (Fig. 5). The algorithm then iterates over several generations, adjusting particle speeds and positions to find an optimal solution. Eqs. (39) and (40) express the particle velocity and position update, respectively [20,25].

$$V_i(t+1) = \chi V_i(t) + c_1 r_1 (P_{best} - x_i(t)) + c_2 r_2 (G_{best} - x_i(t)) \quad (39)$$

$$x_i(t+1) = x_i(t) + v_i(t+1) \quad (40)$$

With c_1 and c_2 representing the cognitive and social parameters which direct the particles towards the best individual (P_{best}) and global (G_{best}) value. Expressed in Eqs. (41) and (42). The terms r_1 and r_2 are random real numbers between 0 and 1 [22].

$$c_1 = \chi\varphi_1 \quad (41)$$

$$c_2 = \chi\varphi_2 \quad (42)$$

Where the term χ makes it possible to improve the convergence called constriction coefficient.

Table 2 presents the different input data that are used.

2.4.3. Optimal selection algorithm

Previous studies are generally limited to maximizing energy performance, thereby minimizing other performance criteria. Thus, in this study, each objective function is either maximized or minimized and are all equivalent in decision making. It should be noted that these priorities are based on the needs sought by the designer. Fig. 5 thus presents the optimal selection network of the best PV/T system.

3. Results and discussion

3.1. Validation

The different configurations are validated in Table 3. This is to check whether the simulation models are able to accurately reproduce reality. A comparison is made between our electrical, thermal and exergetic efficiencies and those obtained in the literature. The average efficiencies

Table 3
Validations of simplified PV/T models.

Reference	Settings	Features	Electrical efficiency (%)	Thermal efficiency (%)	Exergetic efficiency (%)
Present work	PV/T-PCM/Air	$\rho_{s,pcm}$	11.09	34.2	18.1
[36]		$= 880 kg/m^3$; $\rho_{l,pcm} = 770 kg/m^3$	10.6	33.2	17.4
RE (%)			4.62	3.01	4.02
Present work	PV/T-PCM/W	$m = 500$ kg/s	13.1	51.23	–
[39]			13.22	49	–
RE (%)			0.9	4.55	–
Present work	BPV/T-Air	$P = 0.66$	9.19	48.53	–
[37]			8.92	47.24	–
RE (%)			3.02	2.73	–
Present work	PV/TW	$G = 1000$ W/m^2	11.38	70.12	–
[38]			12.07	69.1	–
RE (%)			5.71	1.47	–
Present work	PV/T-Air	$T_a = 46.3$ °C	12.4	24.5	14.3
[7]			13.16	23.24	13.97
RE (%)			5.77	5.42	2.36
Present work	PV/T-TNF	Volume fraction (1 %)	13.39	60	–
[24]			13.54	58.8	–
RE (%)			1.1	2.04	–
Present work	PV/T-TEG/Air	$\dot{m} = 0.05$ kg/s	12	62.73	–
[13]			12.7	66.6	–
RE (%)			5.51	5.81	–

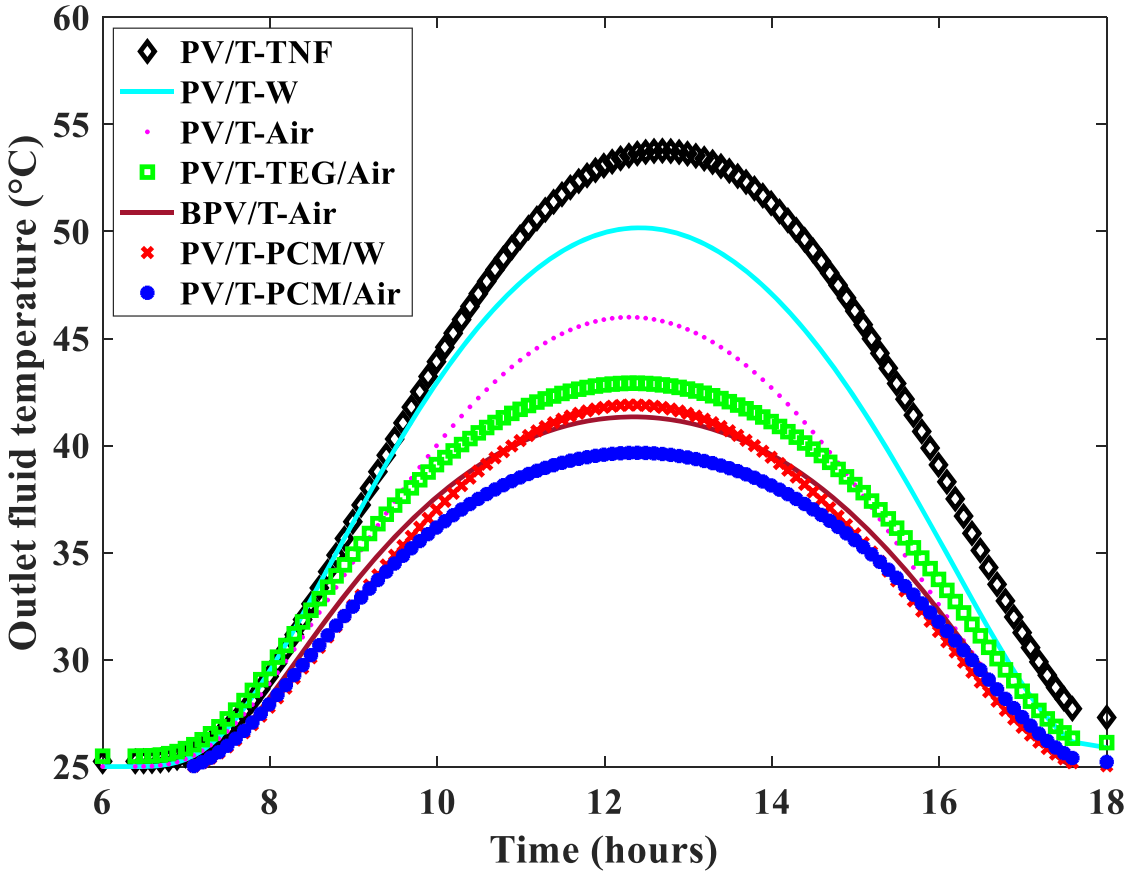

Fig. 6. Temporal evolution of the temperature of the fluids at the outlets.

are compared with each other as well as the maximum efficiencies for each model of identical configurations. Similarly, the characteristics of each model are taken to be identical for a fair comparison.

It can be observed in Table 3 that the relative error for each model is less than 6 %. This demonstrates the reliability of simplified PV/T models. Proving their usefulness for the simulation of PV/T systems.

3.2. Evaluation of performances

3.2.1. Outlet fluid temperatures

Fig. 6 shows the temporal variation of the temperature of the fluids released for one day. These models are simulated using the Capderou solar radiation estimation model [35]. A volume concentration of 1 % is used for the case of the PV/T-TNF model with a common flow rate of 8 %. The temperature of the fluids at the outlets is maximum between 12

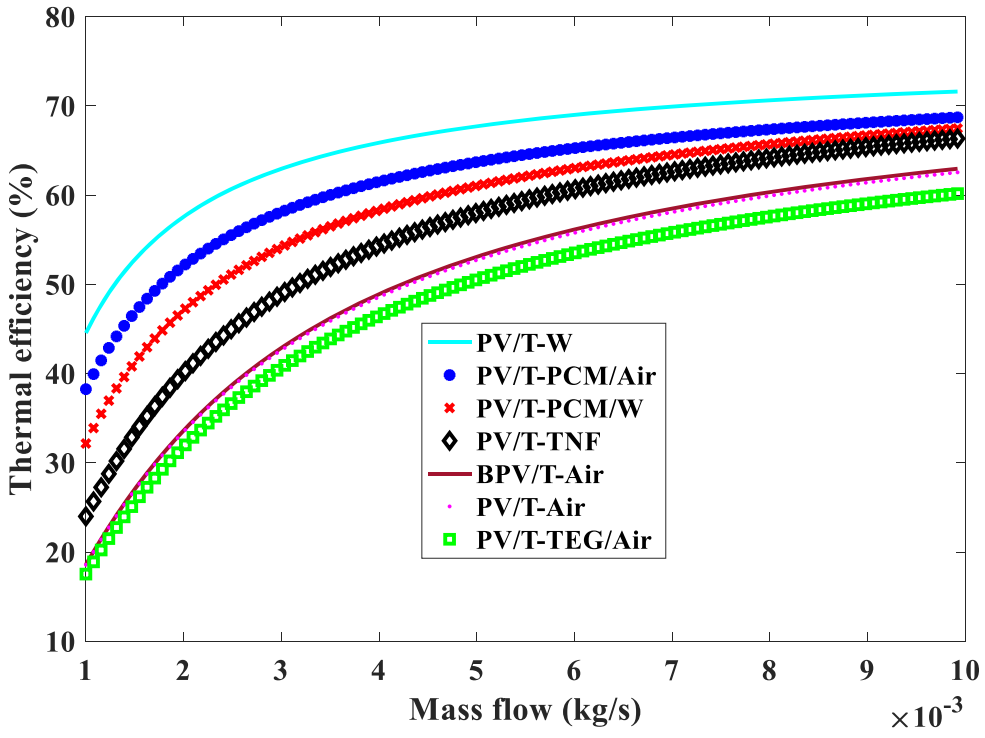

Fig. 7. Thermal efficiency as a function of mass flow.

p.m.−1 p.m. which corresponds to the time of maximum solar irradiation. Active liquid cooling systems rise in temperature more quickly than air systems and reach the highest values near solar noon. The evolution of temperatures with air systems is therefore clearly differentiated, with difficulty in dropping its temperature. The intensity of ambient heat being higher in the afternoon makes cooling more difficult for air systems. Also, due to the thermal conductivity of air which is very low compared to water, liquid cooling systems therefore have a better capacity to extract heat from the PV/T components. This reduces the efficiency of the thermal exchanges. A difference is observed for the case of systems with PCM which have low outlet temperatures due to the melting phenomenon which tends to maintain a constant temperature even during intense heat conditions. For TEG systems, they act as an additional heat sink for the PV components. The outlet temperature of PV/T-TEG/Air systems which is 1.25 times lower than that of PV/T-TNF configurations can be justified by the recovery of part of the heat by the TEG for conversion in electricity. This analysis highlights the different physical and thermodynamic mechanisms that govern the behavior of the various types of PV/T systems studied, depending on the cooling technologies used. These results underline the importance of a detailed

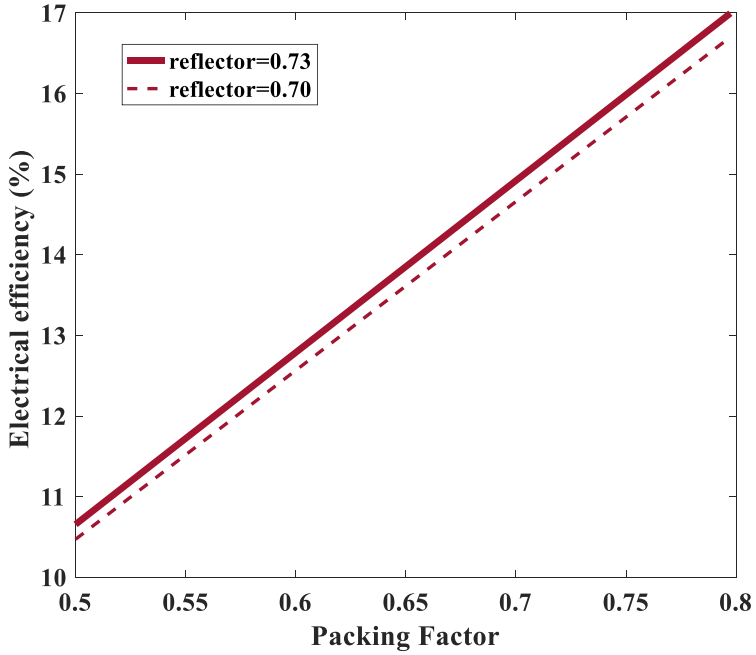

Fig. 8. Evolution of electrical efficiency depending on the packaging factor.

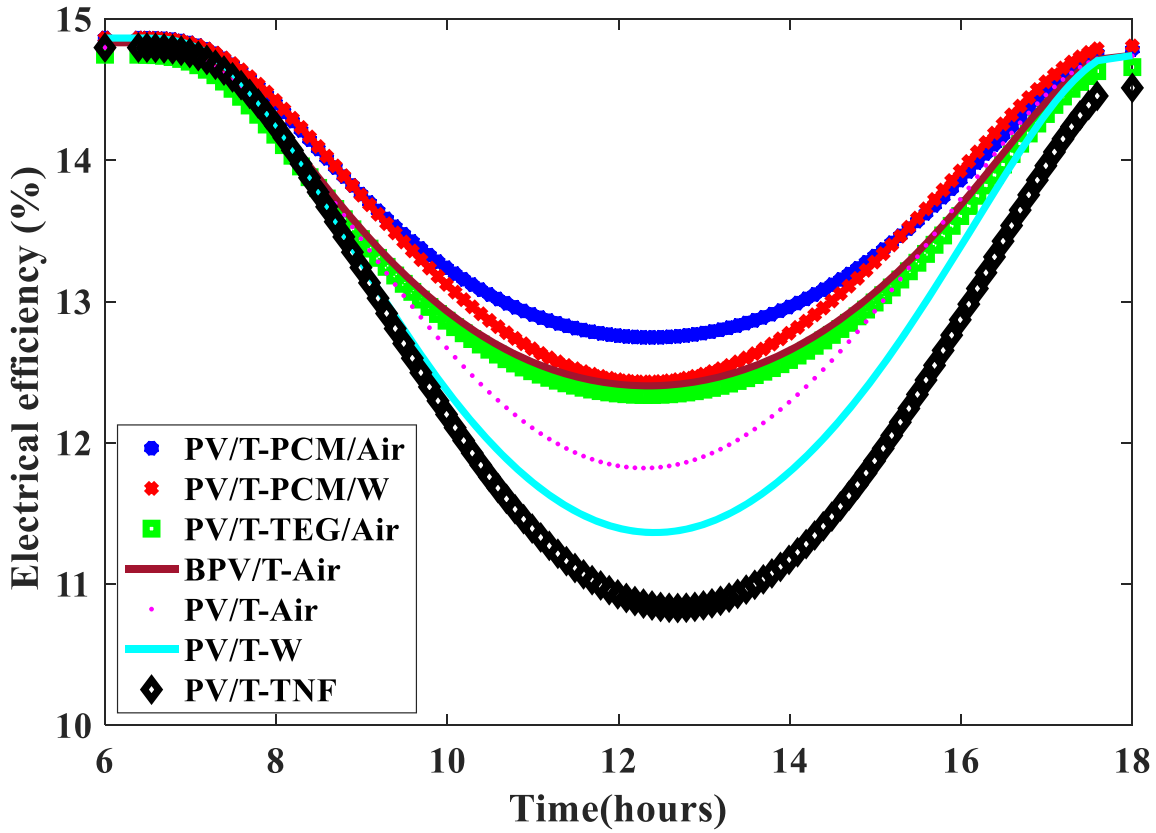

Fig. 9. Electrical efficiency versus time.

understanding of the physical phenomena to optimize the performance of these hybrid systems.

3.2.2. *Thermal efficiencies of configurations*

Solar irradiation is maintained at $G = 800$ W/ m^2 to have a significant thermal flux to be dissipated at the PV/T system level. The ambient temperature is also kept constant at 35 °C and the flow rate varies from $10^{-3}$to 10^{-2}kg/s allowing the observation of the existence of an optimal flow rate that maximizes the thermal efficiency. The appearance of the thermal efficiency of the configurations as a function of the flow rate is presented in Fig. 7. Thermal efficiency increases as a function of flow rate and tends to stabilize at a certain flow rate value. This trend is due to a balance between heat dissipation and the energy demand needed to circulate fluids at a high rate. The PV/TW, PV/T-PCM/Air, PV/T-PCM/W and PV/T-PCM/TNF systems, respectively have a thermal efficiency of 71.62 %, 68.73 %, 67.48 %, 66.35 % at optimal flow. The last 3 are

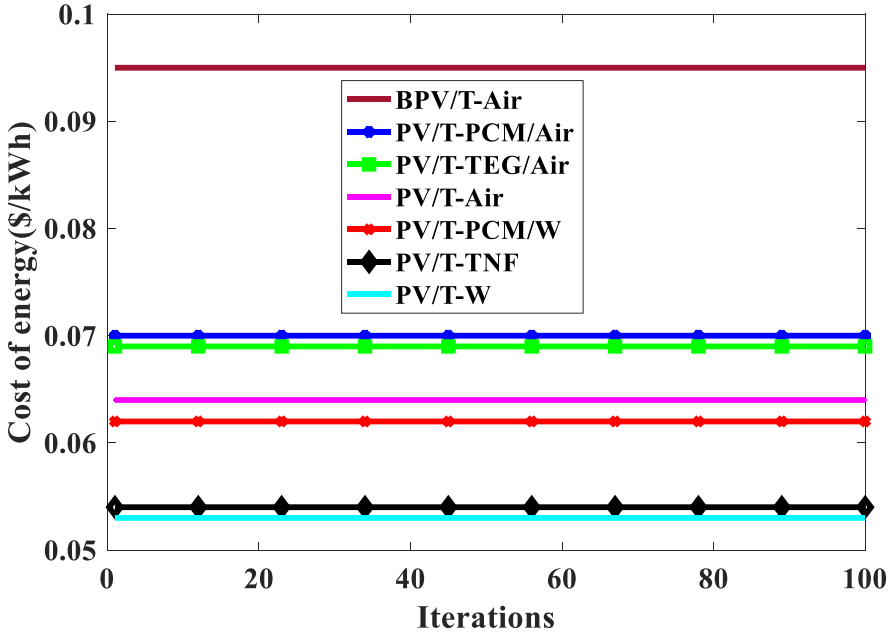

Fig. 10. Convergence of the COE of the different models.

Table 4
: Objective function values obtained.

Models	ENEVEC ($/yr)	EVEC ($/yr)	NPV ($)	COE ($/kWh)	EXEV ($kgco_2/yr$)	SI	ENEV ($kgco_2/yr$)	CPBT (yr)	EXEVEC ($/yr)
PV/T-TNF	0.00014	0.107	569.09	0.054	0.00545	2.13033	0.01006	2.20120	7.91E-05
PV/TW	0.00020	0.108	567.43	0.0533	0.00787	3.31876	0.01424	2.13857	0.00011
PV/T-Air	4.45E-05	0.103	510.26	0.064	0.00165	1.35881	0.00306	2.56465	2.40E-05
PV/T-TEG/Air	7.68E-05	0.102	481.11	0.0697	0.00258	1.49180	0.00529	2.79310	3.75E-05
PV/T-PCM/W	1.71E-04	0.101	494.03	0.062	0.00748	2.63439	0.01177	2.50515	1.08E-04
PV/T-PCM/Air	5.99E-05	0.10	466.64	0.070	0.00314	1.45744	0.00413	2.82891	4.55E-05
BPV/T-Air	4.04E-05	0.102	420.20	0.095	0.00135	1.24173	0.00278	3.80796	1.97E-05

the air configurations including BPV/T-Air, PV/T-Air and PVT/TEG/Air which have a maximum efficiency below 63 %. PCM materials compared to TEG have high capacity and thermal conductivity which may explain their higher efficiency. It is possible that liquid or PCM configurations minimize thermal losses in components better than air or TEG configurations.

3.2.3. Electrical efficiency of BPV/T

BPV/T-Air configurations depend on their geometry which is marked by the packing factor and reflectance of the reflector. Fig. 8 shows the evolution of the electrical efficiency of the BPV/T-Air configuration as a function of the packing factor which refers to the proportion of the total panel area that is occupied by the PV cells. A large packing factor increases the electrical efficiency of the system. Similarly, reflectance refers to the ability of a surface to reflect sunlight to reflect incident sunlight towards the rear side of the PV cells. However, a higher packing factor can also reduce the surface area available for reflection of sunlight to the back side and even increase the heating of the PV cells. It is therefore important to find an optimal balance between packing factor and reflectance to maximize the overall effectiveness of bifacial panels.

3.2.4. Electrical efficiencies of configurations

We maintain the packing factor at 0.66 and the flow rate $m = 0.01$ kg/s, with a reflection capacity evaluated at 0.73. This is to maintain a balance between packing factor and reflectance. The evolution of the daily electrical efficiency of the configurations is presented in Fig. 9. It is marked by a high electricity conversion performance observed with PCM configurations due to their large absorption and thermal storage capacity, TEG with the possibility of heat absorption to provide electricity efficiently and then the bifacial for its double production in front and behind the PV with an air block cooling the latter. Compared to TNF and W models which have the same PV/T geometry with tubes where these fluids circulate and therefore convection losses are generally higher than air models, not contributing effectively to electrical conversion.

3.3. GA/MOPSO optimization results

3.3.1. Convergence of models

Fig. 10 presents the convergence of the COE for each model as a function of the number of iterations. All these configurations converge in less than a few iterations close to zero, indicating the good performance of the GA/MOPSO algorithm in this study. This demonstrates the effectiveness of this GA and MOPSO hybridization to solve the problem of designing optimal systems with reduced time.

3.3.2. Optimal results

The objectives of designers are often very concentrated and fixed. A wide range of parameters so some can be neglected and sometimes prioritized over one or the other. Hence the relevance of such a study. Table 4 presents the different values of the objective functions obtained for each model. We can see that, in terms of net present value (NPV), all of these models are viable. By analyzing the cost of energy, they are on average 4.9 times lower than the price of electricity currently offered in Cameroon. Especially with liquid-cooled systems.

By observing the energo-environmental (ENEV) and exergoenvironmental (EXEV) functions, it is seen that air models such as BPV/T-Air and PV/T-Air have a low environmental impact in the energy production process compared to active systems with liquids which are high in energy, but have a strong environmental impact. This analysis is also valid for the ENEVEC and EXEVEC functions. Best seen in Table 5, which shows the places occupied by the optimal models for each design objective. The BPV/T-Air, PV/T-PCM/Air and PV/T-TEG/Air models have the longest payback times. This could be justified by the fact that systems which are profitable allow the initial investment to be recovered quickly.

Compared to the economic cost of issuing CO_2, they are all less than $0.108/yr. The PV/TW and PV/T-TNF models have the highest emissions which are arguably therefore the complexity of manufacturing such as pipes and pumps can lead to increased emissions from $CO_2$the installation. However, looking at the cost of the energy that will be produced, liquid water and TNF systems are close to being the most accessible to a population in underdeveloped countries.

Compared to the water model, PCM and TEG, the durability index is

Table 5
Optimal model for each design objective.

Functions / Settings	*ENEVEC* ($/yr)	*EVEC* ($/yr)	*NPV* ($)	*COE* ($/kWh)	*EXEV* ($kgco_2/yr$)	*IF*	*ENEV* ($kgco_2/yr$)	*EF*	*CPBT* (yr)	*EXEVEC* ($/yr)	*GA/MOPSO results*
Best PV/T	BPV/T-Air	PV/T-PCM/Air	PV/T-TNF	PV/TW	BPV/T-Air	PV/TW	BPV/T-Air	PV/T-PCM/Air	PV/TW	BPV/T-Air	PV/T-Air
	PV/T-Air	PV/T-PCM/W	PV/TW	PV/T-TNF	PV/T-Air	PV/T-PCM/W	PV/T-Air	PV/TW	PV/T-TNF	PV/T-Air	PV/T-TNF
	PV/T-PCM/Air	BPV/T-Air	PV/T-Air	PV/T-PCM/W	PV/T-TEG/Air	PV/T-TNF	PV/T-PCM/Air	PV/T-PCM/W	PV/T-PCM/W	PV/T-TEG/Air	PV/T-PCM/Air
	PV/T-TEG/Air	PV/T-TEG/Air	PV/T-PCM/W	PV/T-Air	PV/T-PCM/Air	PV/T-TEG/Air	PV/T-TEG/Air	PV/T-TNF	PV/T-Air	PV/T-PCM/Air	PV/T-PCM/W
	PV/T-TNF	PV/T-Air	PV/T-TEG/Air	PV/T-TEG/Air	PV/T-TNF	PV/T-PCM/Air	PV/T-TNF	PV/T-TEG/Air	PV/T-TEG/Air	PV/T-TNF	BPV/T-Air
	PV/T-PCM/W	PV/T-TNF	PV/T-PCM/Air	PV/T-PCM/Air	PV/T-PCM/W	PV/T-Air	PV/T-PCM/W	BPV/T-Air	PV/T-PCM/Air	PV/T-PCM/W	PV/TW
Worst PV/T	PV/TW	PV/TW	BPV/T-Air	BPV/T-Air	PV/TW	BPV/T-Air	PV/TW	PV/T-Air	BPV/T-Air	PV/TW	PV/T-TEG/Air

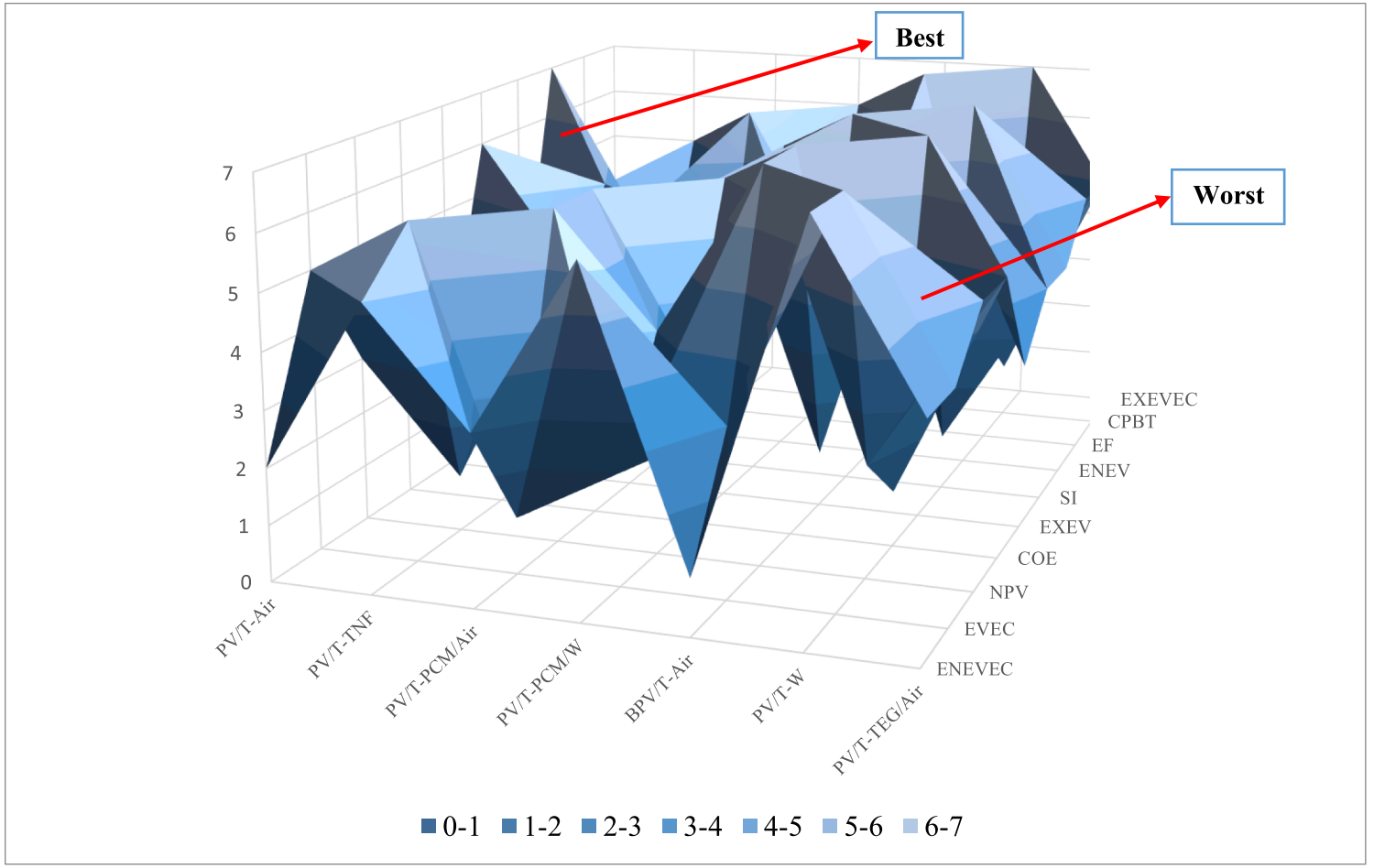

Fig. 11. Fluctuations in the ranks of each PV/T model depending on the design objectives.

remarkable, although their ergonomic factor plays to their disadvantage. PCM systems are central to every design objective. They are better than the bifacial system or the TEG for the search for a less polluting PV/T model and therefore the savings linked to emissions are CO_2 considerable. The GA/MOSPSO hybrid method reveals that the optimal PV/T design balance is achieved with the Air PV/T system (Fig. 11). Air is more compatible with PCM materials than liquids in PV/T systems, as its slower heat transfer rate allows better utilization of the PCM's latent heat storage capacity, thus improving the overall system performance. The latter represents the best compromise in terms of energy and exergy efficiency, environmental impact, and reduced costs. This highlights the interest of air-based solutions, despite their slightly lower performance compared to liquid or PCM configurations. These functions therefore demonstrate maximum energy and exergy efficiency and minimal environmental impact with reduced costs.

4. Conclusion

This study aims to provide a simplified model of seven innovative PV/T systems, notably passive ones with phase change materials (PCM), thermoelectric generators and bifacial; Then active with water, air and ternary nanofluids (TNF) with passive/active hybridization. Thus, the failures encountered by these systems, such that one may be more efficient but less energy-efficient while the other may be less efficient but more energy-efficient with a relevant look at the balance of sustainability and economy, leads to the design of an optimal selection model of the PV/T system for decision making. Thus, a hybrid numerical model using genetic algorithms and multi-objective particle swarm optimization (GA/MOPSO) is implemented. This study takes into account ten objective functions arising from the 10E analysis. In particular the energy-environmental, exergo-environmental, energy-enviro-economic, exergo-enviro-economic, enviro-economic function, energy cost, net present value, sustainability index, return on investment time and the ergonomic factor. We can conclude from this research that:

- Ø The hybridization of the Genetic Algorithm and multiobjective particle swarm optimization method is effective for the selection of optimal systems;
- Ø Liquid cooling systems therefore have a better ability to extract heat from PV/T components than air configurations;
- Ø Air appears to be more compatible with PCM materials than liquids;
- Ø Specifically for BPV/T, a higher packing factor can reduce the surface area available for reflecting sunlight to the back side. Hence the importance of an optimal balance between the packing factor (0.66) and the reflectance (0.7) to maximize the electrical efficiency of bifacial panels at 13.1 % at 800 W/ m^2 ;
- Ø However, the study shows good viability of PV/T models with a Cost of energy and a return on investment time all lower than 0.1$/kWh and 3 years respectively;
- Ø The bifacial model stands out with a good energy-environmental balance compared to the water model which has a better durability index greater than 2 on the other hand with air systems where it is less than 1.5;
- Ø It is possible that liquid or PCM configurations minimize thermal losses in the components better than air or TEG configurations;
- Ø PCM, TEG and bifacial PV/T models feature high electrical efficiency;
- Ø air models such as BPV/T-Air and PV/T-Air have a low environmental impact in the energy production process compared to active systems with liquids which are high in energy;
- Ø PV/T models with TNF and W have higher convection losses than air models, not contributing effectively to electrical conversion;
- Ø The GA/MOSPSO hybrid method reveals that the optimal PV/T design balance is achieved with the Air PV/T model.

This study is of capital importance because it highlights the influence of each PV/T model on several axes. Allowing designers and decision-makers to be better informed. This selection method can be extended to all renewable energy technologies. As a perspective, this research could be pushed forward by carrying out a selective study of the type of PV cells among the existing and new multitudes such as perovskites in different configurations and by exploring other optimization methods.

Funding statement

This research did not receive any specific grant from funding agencies in the public, commercial, or not-for-profit sectors.

Data availability statement

We have included the data sources in the manuscript.

CRediT authorship contribution statement

Armel Zambou Kenfack: Writing – review & editing, Writing – original draft, Visualization, Validation, Supervision, Software, Resources, Project administration, Methodology, Investigation, Funding acquisition, Formal analysis, Data curation, Conceptualization. **Modeste Kameni Nematchoua:** Writing – original draft, Visualization, Validation, Supervision, Software, Resources, Formal analysis, Data curation, Conceptualization. **Elie Simo:** Writing – original draft, Visualization, Validation, Supervision, Software, Resources, Formal analysis. **Venant Sorel Chara-Dackou:** Visualization, Validation, Supervision, Software, Resources, Project administration, Formal analysis, Conceptualization. **Boris Abeli Pekarou Pemi:** Writing – original draft, Visualization, Validation, Supervision, Software, Project administration, Funding acquisition.

Declaration of competing interest

The authors declare that they have no known competing financial interests or personal relationships that could have appeared to influence the work reported in this paper.

References

[1] A. Mohammad, F. Mahjabeen, Revolutionizing solar energy: the impact of artificial intelligence on photovoltaic systems, Int. J. Multidiscip. Sci. Arts 2 (1) (2023), https://doi.org/10.47709/ijmdsa.v2i1.2599.
[2] A. Mohammed, P. Bencs, Energy and exergy analysis for photovoltaic modules cooled by evaporative cooling techniques, Energy Rep. 9 (2023) 122–132, https://doi.org/10.1016/j.egyr.2022.11.177.
[3] C. Yuanlong, Z. Jie, Z. Fan, S. Yiming, X. Yibing, Current status and future development of hybrid PV/T system with PCM module: 4E (energy, exergy, economic and environmental) assessments, Renew. Sustain. Energy Rev. (2022), https://doi.org/10.1016/j.rser.2022.112147, 158; 112147.
[4] H. María, W. Kai, H. Gan, Ot Todd, B.M. Osama, A.A. Rafaela, D. Yulong, K. Soteris, N. Ekins-Daukes, R.A. Taylor, C.N. Markides, A review of solar hybrid photovoltaic-thermal (PV-T) collectors and systems, Prog. Energy Combust. Sci. 97 (2023) 101072, https://doi.org/10.1016/j.pecs.2023.101072. ISSN 0360-1285.
[5] W.J. Aruldoss, S. Padmini, C. Bharatiraja, Performance studies of a solar thermal-electric hybrid desalination system: 4E (energy-exergy-economics-enviroeconomics) analysis, Environ. Sci. Pollut. Res. 30 (2023) 73451–73468, https://doi.org/10.1007/s11356-023-27938-7.
[6] K. Amirhooshang, R.A. Fatemeh, M.H. Mohammad, A.V.R. Mohammad, Experimental investigation of a PV/T system containing a TEG section between water-based heat exchanger and air-based heat sink, Therm. Sci. Eng. Prog. 42 (2023) 101909, https://doi.org/10.1016/j.tsep.2023.101909. ISSN 2451-9049.
[7] S.S. Ahmed, 4E analysis of a new design heat sink for cooling a bifacial photovoltaic system using PCM and ribs, J. Energy Storage 73 (Part B) (2023) 108907, https://doi.org/10.1016/j.est.2023.108907. ISSN 2352-152X.
[8] Z. Xuanxun, C. Xiaoling, L. Ziyu, Z. Xu, L. Silin, Study on the temperature control performance of photovoltaic module by a novel phase change material/heat pipe coupled thermal management system, J. Energy Storage 64 (2023) 107200, https://doi.org/10.1016/j.est.2023.107200. ISSN 2352-152X.
[9] G. Ramadan, M. Hatem, O. Shinichi, H. Hamdy, Energy, exergy, and economic assessment of thermal regulation of PV panel using hybrid heat pipe-phase change material cooling system, J. Clean. Prod. 364 (2022) 132489, https://doi.org/10.1016/j.jclepro.2022.132489. ISSN 0959-6526.

[10] M.T. Chaichan, H.A. Kazem, M.K. Al-Ghezi, A.H. Al-Waeli, A.J. Ali, K. Sopian, A. A Al-Amiery, Effect of different preparation parameters on the stability and thermal conductivity of MWCNT-based nanofluid used for photovoltaic/thermal cooling, Sustainability 15 (9) (2023) 7642, https://doi.org/10.3390/su15097642.
[11] B. Mehta, D. Subhedar, H. Panchal, Z. Said, Synthesis, stability, thermophysical properties and heat transfer applications of nanofluid–A review, J. Mol. Liq. (2022) 120034, https://doi.org/10.1016/j.molliq.2022.120034.
[12] K.A. Zambou, M.K. Nematchoua, E. Simo, M.N. Mfoundikou, J.V.K. Fosso, M. H. Babikir, V.S. Chara-Dackou, Exergetic optimization of some design parameters of the hybrid photovoltaic/thermal collector with bi-fluid air/ternary nanofluid (CuO/MgO/TiO $_2$), SN. Appl. Sci. 5 (8) (2023) 226, https://doi.org/10.1007/s42452-023-05455-z.
[13] S. Mukherjee, V. Poloju, P.C. Mishra, Heat transfer, exergoeconomic performance and sustainability impact of a novel CuO+ MgO+ GO/Water ternary nanofluid, Appl. Therm. Eng. 235 (2023) 121391, https://doi.org/10.1016/j.applthermaleng.2023.121391.
[14] O. Poorya, S. Kamaruzzaman, H.Z. Saleem, Z. Rozli, Performance of four air-based photovoltaic thermal collectors configurations with bifacial solar cells, Renew. Energy (2016), https://doi.org/10.1016/j.renene.2016.10.043.
[15] F. Ahmad, M. Muslizainun, T. Ivan, A. Fitrotin, A.G. Koto, K. Sopian, Photovoltaic thermal (PVT) air collector with monofacial and bifacial solar cells: a review, Int. J. Power Electr. Drive Syst. 10 (4) (2019) 2021–2028, https://doi.org/10.11591/ijpeds.v10.i4.pp2021-2028.
[16] J. Joji, S. Manikandan, Experimental study and model development of bifacial photovoltaic power plants for Indian climatic zones, Energy 284 (2023) 128693, https://doi.org/10.1016/j.energy.2023.128693.
[17] A.J. Cetina-Quinones, I. Polanco-Ortiz, M.A. Pedro, J.G. Hernandez-Perez, A. Bassam, Innovative heat dissipation design incorporated into a solar photovoltaic thermal (PV/T) air collector: an optimization approach based on 9E analysis, Therm. Sci. Eng. Prog. 38 (2023) 101635, https://doi.org/10.1016/j.tsep.2022.101635, 2451-9049.
[18] Y. Noorollahi, A.G. Nani, A. Fadaei, S. Mobina, S. Rahim, A framework for GIS-based site selection and technical potential evaluation of PV solar farm using Fuzzy-Boolean logic and AHP multi-criteria decision-making approach, Renew. Energy 186 (2022) 89–104, https://doi.org/10.1016/j.renene.2021.12.124.
[19] S.B. Mousavi, M.H. Nabat, A.R. Razmi, P Ahmadi, A comprehensive study and multi-criteria optimization of a novel sub-critical liquid air energy storage (SC-LAES), Energy Convers. Manage 258 (2022) 115549, https://doi.org/10.1016/j.enconman.2022.115549.
[20] bubakar, A., Borkor, R.N., & Amoako-Yirenkyi, P. Stochastic optimal harmonic suppression with permissible photovoltaic penetration level for grid-linked systems using Monte Carlo-Based Hybrid NSGA2-MOPSO. 2023. 10.21203/rs.3.rs-3272851/v1.
[21] Y. Li, Z. Xie, S. Yang, Z. Ren, A hybrid algorithm based on NSGA-II and MOPSO for multi-objective designs of electromagnetic devices, IEEE Trans. Magn. 59 (5) (2023) 1–4, https://doi.org/10.1109/TMAG.2023.3250319.
[22] R. Cheraghi, M.H Jahangir, Multi-objective optimization of a hybrid renewable energy system supplying a residential building using NSGA-II and MOPSO algorithms, Energy Convers. Manage 294 (2023) 117515, https://doi.org/10.1016/j.enconman.2023.117515.
[23] A. Behera, P.S. Kulkarni, Smart temperature-dependent cooling of solar panel using Arduino, in: Proceedings of the 2nd International Conference on Paradigm Shifts in Communications Embedded Systems, Machine Learning and Signal Processing (PCEMS), Nagpur, India, 2023, pp. 1–6, https://doi.org/10.1109/PCEMS58491.2023.10136058.
[24] H. Adun, A. Michael, D. Mustafa, B. Olusola, S. Mehmet, K. Ravinder, A numerical and exergy analysis of the effect of ternary nanofluid on performance of Photovoltaic thermal collector, J. Therm. Anal. Calorim. (2021) 1413–1429, https://doi.org/10.1007/s10973-021-10575-y, flight. 145.
[25] T.H. Djeudjo, D. Njomo, K.F.A. Talla, R. Tchinda, Techno-economic and environmental feasibility study with demand-side management of photovoltaic/wind/hydroelectricity/battery/diesel: a case study in Sub-Saharan Africa, Energy Convers. Manage 258 (2022) 0196–8904, https://doi.org/10.1016/j.enconman.2022.115494.
[26] J. Xinyu, L. Huawei, P. Maoqing, L. Wenzhi, L. Jianqing, L. Dongxue, J Xing, Xu Chao, Multi-parameter study and genetic algorithm integrated optimization for a nanofluid-based photovoltaic/thermal system, Energy 267 (2023) 126528, https://doi.org/10.1016/j.energy.2022.126528.
[27] M.H. Moghaddam, M. Karami, Thermohydraulic optimization of artificial roughness in photovoltaic-thermal (PVT) system using genetic algorithm, J. Build. Eng. 65 (2023) 105789, https://doi.org/10.1016/j.jobe.2022.105789.
[28] D.T. Hermann, K.F.A. Talla, R. Tchinda, D. Njomo, Consideration of some optimization techniques to design a hybrid energy system for a building in Cameroon, Energy Built Environ. 3 (2) (2022) 233–249, https://doi.org/10.1016/j.enbenv.2021.01.007.
[29] R. LI, J. LI, J. Zhu, et al., A numerical and experimental study on a novel micro heat pipe PV/T system, Energy 282 (2023) 128746, https://doi.org/10.1016/j.energy.2023.128746.
[30] M.I. Hussain, K. Jun-Tae, sustainability performance evaluation of photovoltaic/thermal (PV/T) system using different design configurations, Sustainability 12 (2020) 22–9520, https://doi.org/10.3390/su12229520.
[31] K. Zakariya, U.R. Ateekh, Selection of a photovoltaic panel cooling technique using multi-criteria decision analysis, Appl. Sci. 13 (2023) 1949, https://doi.org/10.3390/app13031949.
[32] M.S. Hossain, A.K. Pandey, J. Selvaraj, N.A. Rahim, M.M. Islam, V.V. Tyagi, Two side serpentine flow based photovoltaic-thermal-phase change materials (PVT-PCM) system: energy, exergy and economic analysis, Renew. Energy 136 (2019) 1320–1336, https://doi.org/10.1016/j.renene.2018.10.097.
[33] W.E. EWE, F. Ahmad, S. Kamaruzzaman, A Nilofar, Modeling of bifacial photovoltaic-thermal (PVT) air heater with jet plate, Int. J. Heat Technol. 39 (4) (2021) 1117–1122, https://doi.org/10.18280/ijht.390409.
[34] N.S. Nazri, A. Fudholi, B. Bakhtyar, C.H. Yen, Energy economic analysis of photovoltaic–thermal-thermoelectric (PVT-TE) air collectors, Renew. Sustain. Energy Rev. 92 (2018) 187–197, https://doi.org/10.1016/j.rser.2018.04.061.
[35] V.S. Chara-Dackou, D. Njomo, R. Tchinda, M.H. Babikir, Y.S. Kondji, Thermal performance analysis of the parabolic trough solar collector in the sub-Saharan climate of the central African Republic, Sustain. Energy Technol. Assess. 58 (2023) 103331, https://doi.org/10.1016/j.seta.2023.103331.
[36] R. Tariq, J. Xamán, A. Bassam, L.J. Ricalde, M.A.E. Soberanis, Multidimensionalassessment of a photovoltaic air collector integrated phase changing material considering Mexican Climatic conditions, Energy (2020), https://doi.org/10.1016/j.energy.2020.118304.
[37] A. Fudholi, M. Mustapha, Mathematical modeling of bifacial photovoltaic-thermal (BPVT) collector with mirror reflector, Int. J. Renew. Energy Res. (IJRER) 10 (2) (2020) 654–662.
[38] A.K. Azad, Parvin Salma, Photovoltaic thermal (PV/T) performance analysis for different flow regimes: a comparative numerical study, Int. J. Thermofluids 18 (2023) 100319, https://doi.org/10.1016/j.ijft.2023.100319.
[39] S. Alsaqoor, A. Alqatamin, A. Alahmer, Z. Nan, Y. Al-Husban, H. Jouhara, The impact of phase change material on photovoltaic thermal (PVT) systems: a numerical study, Int. J. Thermofluids 18 (2023) 100365, https://doi.org/10.1016/j.ijft.2023.100365.
[40] V.S. Chara-Dackou, D. Njomo, R. Tchinda, Y.S. Kondji, D.R.K. Legue, Babikir MH Estimation of solar radiation and feasibility analysis of a concentrating solar power plant in Birao, Central African Republic, Int. J. Heat Technol. 41 (6) (2023) 1627–1638, https://doi.org/10.18280/ijht.410626.
[41] A.Z. Kenfack, K.M. Nematchoua, E. Simo, F.A.T. Konchou, M.H. Babikir, B.A. P. Pemi, V.S Chara-Dackou, Techno-economic and environmental analysis of a hybrid PV/T solar system based on vegetable and synthetic oils coupled with TiO2 in Cameroon, Heliyon (2024) e24000, https://doi.org/10.1016/j.heliyon.2024.e24000.
[42] B.A.P. Pemi, D. Njomo, R. Tchinda, J.C. Seutche, A.Z. Kenfack, M.H. Babikir, V. S Chara-Dackou, Sectoral assessment of the energy, water, waste and land nexus in the sustainability of agricultural products in Cameroon, Sustainability 16 (2) (2024) 565, https://doi.org/10.3390/su16020565.
[43] V.S. Chara-Dackou, D. Njomo, R. Tchinda, Y.S. Kondji, H.M. Babikir, N. H. Chopkap, B.A.P. Pemi, A.Z. Kenfack, N.I. Mbouombouo, Sensitivity analysis of the thermal performance of a parabolic trough concentrator using Al2O3 and SiO2/Vegetable oil as heat transfer fluid, Heliyon (2024) e23978, https://doi.org/10.1016/j.heliyon.2024.e23978. ISSN 2405-8440.